JOC The Journal of Organic Chemistry

Article

pubs.acs.org/joc

# Mechanism and Selectivity in the Pd-Catalyzed Difunctionalization of Isoprene

Liping Xu,[†,∥,#] Xin Zhang,[†,#] Matthew S. McCammant,[⊥] Matthew S. Sigman,[⊥] Yun-Dong Wu,[†,‡] and Olaf Wiest*[,§]

[†]Laboratory of Computational Chemistry and Drug Design, Laboratory of Chemical Genomics, Peking University Shenzhen Graduate School, Shenzhen 518055, People's Republic of China

[∥]School of Chemical Engineering, Shandong University of Technology, Zibo 255049, People's Republic of China

[⊥]Department of Chemistry, University of Utah, 315 S. 1400 East, Salt Lake City, Utah 84112, United States

[‡]College of Chemistry and Molecular Engineering, Peking University, Beijing 100871, People's Republic of China

[§]Department of Chemistry and Biochemistry, University of Notre Dame, Notre Dame, Indiana 46556-5670, United States

Supporting Information

**ABSTRACT:** The three-component coupling of isoprene, an alkenyl triflate, and styrenylboronic acid catalyzed by a palladium pyrox complex affords access to skipped dienes from simple chemical feedstocks. Unfortunately, the transformation proceeds with only moderate selectivity and yields. The reaction mechanism and factors responsible for the resulting regioselectivity were elucidated using M06/SDD/6-311++G(d,p) + SMD calculations. Distortion of the palladium coordination sphere in the transition structure of the migratory insertion step is found to control the 4,1- vs 1,*x*-selectivity. The calculated $\Delta\Delta G^{\ddagger}$ of 1.0 kcal/mol for this step is in excellent agreement with the experimentally observed selectivity of 1:9.9 disfavoring the 4,1-product. The transmetalation was found to be the regioselectivity determining step for the formation of the 1,2- vs 1,4-addition products. Systematic conformational searches for the transmetalation transition structure revealed a series of steric interactions between the *t*-Bu substituent on the ligand and the substrates in the model system that are balanced by additional repulsive interactions between the substrates and the pyridyl portion of the ligand. The combination of these effects leads to the low to moderate 1,2- vs 1,4-selectivity in the experimentally studied system.

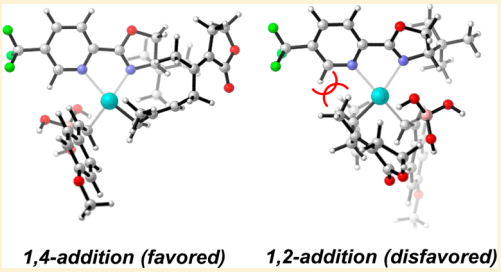


## INTRODUCTION

Palladium-catalyzed difunctionalization of alkenes has attracted much attention in recent years because it provides access to a broad range of structurally diverse functionalized chemicals and is considered a powerful strategy in synthetic organic chemistry.[1−3] The range of these reactions can be further expanded by functionalization of 1,3-dienes with the three-component coupling strategy shown in Figure 1. Trans-

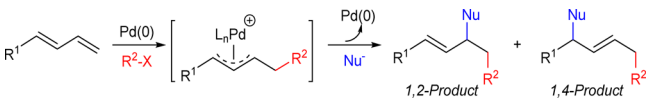


**Figure 1.** Pd(0)-catalyzed difunctionalization of 1,3-dienes.

formations of this type are economically very attractive because they employ easily accessible chemical feedstocks such as butadiene or isoprene.[4] McCammant et al. demonstrated that 1,4-difuctionalization of dienes by aryl and vinyl groups provides efficient access to skipped polyenes, a common but challenging structural element to access in many natural products.[5−10] Similarly, Gong and co-workers demonstrated that stereoselective 1,2-alkene difunctionalization through the formation of $sp^2$ and $sp^3$ carbons is possible.[11] The formation of a wide range of different products in these Pd-catalyzed difunctionalization reactions suggests that a detailed understanding of the relevant structural and electronic origins could be used to improve the moderate selectivity often observed when unsymmetrical 1,3-dienes are utilized.

To understand the relevant selectivities observed for the various products of 1,3-diene difunctionalization, the individual steps of the proposed mechanism shown in Figure 2 must be carefully considered. A Pd(0) complex undergoes initial oxidative addition with $R^2$-X, which undergoes subsequent migratory insertion of a 1,3-diene to form a Pd(II)-alkyl complex (**III** in Figure 2). This species could either react directly with a cross-coupling partner to form a 1,2-addition product or proceed through an $\sigma-\pi-\sigma$ isomerization to give $\sigma$-allyl intermediate **V**. The 1,4-addition product **VII** is formed after boronic acid transmetalation at palladium and subsequent reductive elimination. Formation of $\pi$-allyl Pd-species **IV** is therefore a key step for the bifurcation between the formation of 1,2- and 1,4-addition products. The experimental data

**Received:** June 1, 2016
**Published:** August 3, 2016




DOI: 10.1021/acs.joc.6b01317
J. Org. Chem. 2016, 81, 7604−7611

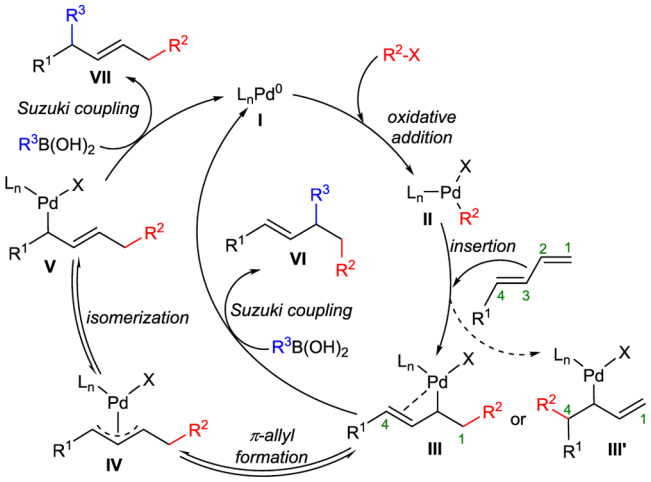


**Figure 2.** Mechanistic pathways of the Pd(0)-catalyzed difunctionalization of 1,3-dienes.

suggest that this selectivity is largely controlled by the steric influence of the $R^1$-group on the $\pi$-allyl stabilized Pd-intermediate.[5−10] When $R^1$ is a sterically encumbering group, complex **V** is unstable due to the repulsion between palladium and $R^1$. This influence causes a reversion of the $\pi$-allyl species **IV** to **III**, thus ultimately leading to the formation of the 1,2-addition product **VI**.[5,6,9,10] If $R^1$ is a relatively small group (i.e., H), complex **V** is more stable and the reaction will proceed to selectively form the 1,4-addition product (Figure 2).[7] Furthermore, if $R^1$ is a relatively small group, the initial migratory insertion step could occur from the internal double bond (between $C_3$ and $C_4$) to form intermediate **III′**. If this pathway were operative, the formation of 4,1-addition products would also be expected.

Recently, the palladium-catalyzed 1,4-difunctionalization of isoprene using pyridine-oxazoline (pyrox) ligands shown in Figure 3 was disclosed.[8] Here, an alkenyl triflate and a

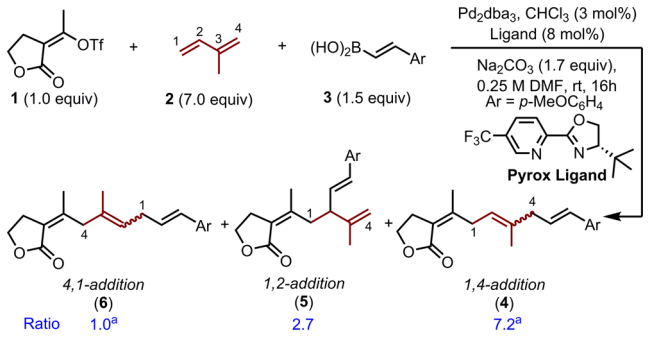


[a]Only the major (*E*)-isomer is taken into consideration.

**Figure 3.** Pd-catalyzed difunctionalization of isoprene.

styrenylboronic acid are coupled in a three-component reaction with isoprene to give mixtures of 1,4-, 1,2-, and 4,1-addition products with moderate selectivity and yields. Multidimensional correlation analysis of the observed product distributions indicated that the site selectivity of alkene insertion correlates linearly with Sterimol $B_1$ values, while the selectivity between 1,4 vs 1,2-addition correlates with the Hammett $\sigma$-values of the pyrox ligands. Obviously, these statistical correlations do not provide the physical origin of the observed product distributions or provide insights into the geometric and electronic structure of the relevant transition structures. In the present manuscript, we investigate the mechanism of the isoprene difunctionalization catalyzed by palladium-pyrox complexes using DFT methods. Elucidation of the different mechanistic pathways provides the structural and electronic origins of the experimentally observed regioselectivity between 1,2-, 1,4-, and 4,1-addition products.

## COMPUTATIONAL DETAILS

All geometry optimizations were performed using the M06 functional[12,13] as implemented in Gaussian 09.[14] This functional includes corrections for dispersion interactions and was found to be reliable for studies of Pd-catalyzed Heck[15−17] and related reactions.[11,18] The Lanl2DZ[19] and ECP (augmented with one f function,[20] Pd($\zeta_f$) = 1.472) as well as 6-31G(d,p) basis sets were used for Pd and all other atoms, respectively. Frequency calculations at the same level of theory as the geometry optimizations were carried out to confirm stationary points as either minima (zero imaginary frequency) or transition structures (one imaginary frequency). Single point calculations using the SDD basis set[21] for Pd and the 6-311++G(d,p) basis set for all other atoms together with the SMD[22] implicit solvent model with the parameters for DMF were used to account for solvent effects. The final free energies from the single point calculations with solvent and thermal corrections are reported in kcal/mol. Images of the optimized structures were prepared using CYLview.[23]

## RESULTS AND DISCUSSION

**Overall Catalytic Cycle.** The overall reaction pathway for the Pd-catalyzed difunctionalization of isoprene depicted in Figure 4 begins with the oxidative addition of an alkenyl triflate

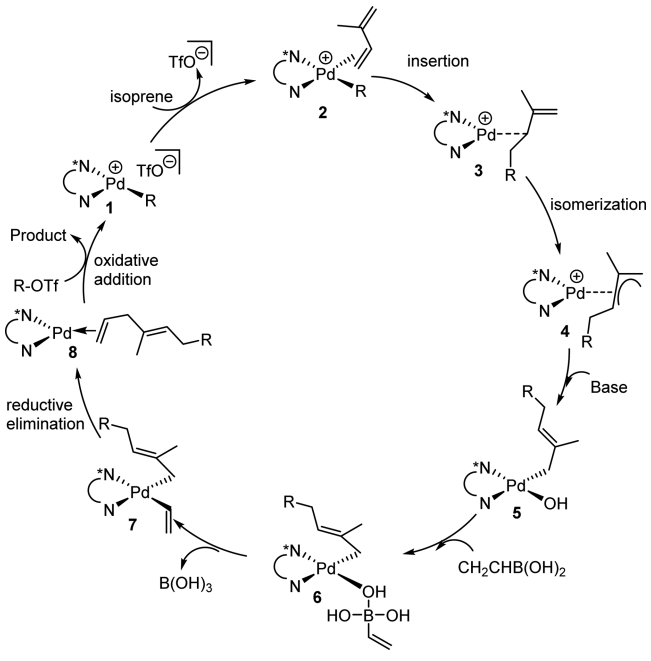


**Figure 4.** Proposed catalytic cycle of the Pd-catalyzed three-component coupling reaction.

(ROTf) to form **1**, followed by coordination of isoprene to palladium, which has been studied previously (**2**, Figure 4).[16] Following alkene migratory insertion, $\sigma-\pi$ isomerization results in the formation of the $\pi$-allyl stabilized Pd-intermediate **4**. Base ($OH^-$) promoted isomerization, promoted by hydroxide, formed through decomposition of sodium carbonate, and coordination of the alkenyl boronic acid generates Pd-complex



DOI: 10.1021/acs.joc.6b01317
J. Org. Chem. 2016, 81, 7604−7611

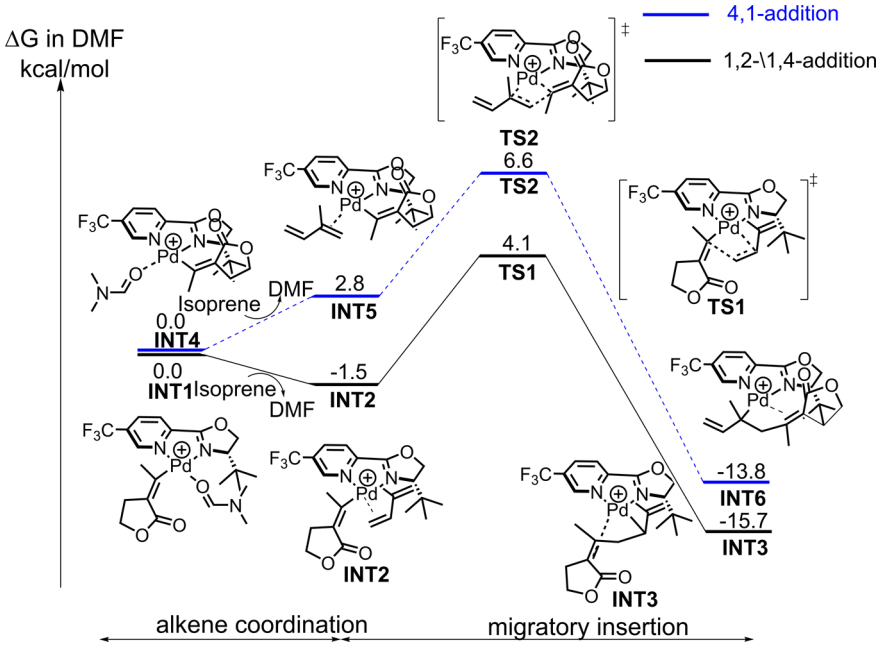


**Figure 5.** Alkene coordination and migratory insertion steps for the pathways leading to 1,*x*- and 4,1-addition.

**6**. Transmetalation of the coordinated boronic acid yields complex **7**, which subsequently undergoes reductive elimination to generate the product-bound palladium intermediate **8**. The catalytic cycle is completed with the substitution of R-OTf and the dissociation of product. The individual sections of this catalytic cycle responsible for the observed product selectivity will be discussed further below.

**1,*x*- vs 4,1-Addition (*x* = 2 or 4).** The initial alkene insertion step from **1** to **2** determines the selectivity in the formation of the **4**/**5** or **6**. While steric effects would favor attack on $C_1$, electronics favors attack on the more electron-rich $C_4$ position. In the absence of a ligand, alkene insertion to either the $C_1$ or $C_4$ position of isoprene was shown to be virtually unselective for the system studied here (**4**/**5**:**6**, 2:1).[8] Alternatively, in the presence of a *t*-Bu pyrox ligand, the same regioselectivity increases to 9.9:1, favoring the formation of intermediates **4**/**5**.

To elucidate the factors responsible for these results, the pathways for alkene coordination and the migratory insertion were calculated. This work is rendered more complex by the asymmetry of all three components of the reaction: diene, alkenyl triflate, and pyrox ligand. To account for the asymmetry of the Pd-intermediates, the calculation of 16 migratory insertion transition structures (TS) was necessary (see Figure S1 in the Supporting Information). Figure 5 displays the mechanistic pathways starting from the lowest-energy structures leading to the 1,*x*- and 4,1-addition, respectively.

The pathways start with **INT1** and **INT4**, where the alkenyl group is in *trans* or *cis* position to the oxazoline portion of the bidentate ligand, respectively. For **INT1**, DMF is replaced by isoprene to form **INT2** with a free energy of binding of $\Delta G$ = −1.5 kcal/mol. Subsequently, the migratory insertion step occurs through **TS1** ($\Delta G^{\ddagger}$ = 4.1 kcal/mol relative to **INT1**) to form intermediate **INT3** with a $\Delta G$ = −15.7 kcal/mol. This intermediate can in subsequent steps lead to either the 1,2- or the 1,4-addition product, as will be discussed below. The activation barrier of the insertion step from **INT2** is 5.6 kcal/mol. For **INT4**, the ligand exchange step to **INT5** is slightly endothermic with a free energy of 2.8 kcal/mol. The transition structure **TS2** for the migratory insertion step leading to the 4,1-addition precursor **INT6** has a free energy of activation of $\Delta G^{\ddagger}$ of 6.6 kcal/mol, and **INT6** is accessed with a $\Delta G$ = −13.8 kcal/mol. If the exchange of isoprene and DMF is, in analogy to earlier studies,[16] rapid, then the Curtin−Hammett principle would be applicable. The barriers of the migratory insertion step are 5.6 and 8.1 kcal/mol for the 1,*x*-addition pathway and the 4,1-addition pathway, respectively. In this scenario, the calculated differences in free energy of activation are within 2.5 kcal/mol and are modestly higher than what would be expected based on the experimentally observed regioselectivity (9.9:1). Alternatively, a non-Curtin−Hammett scenario would lead to a $\Delta\Delta G^{\ddagger}$ of 1.0 kcal/mol and is in excellent agreement with experimental observations. However, both scenarios are plausible within the computational uncertainty.

Figure 6 shows the geometries of the two selectivity determining transition structures **TS1** and **TS2**. Interestingly,

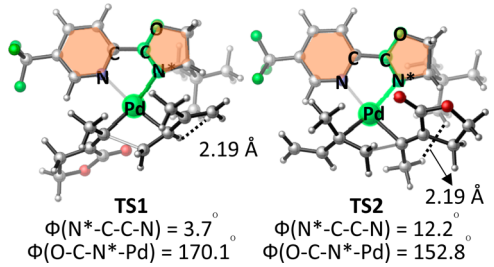


**Figure 6.** Geometries of **TS1** and **TS2**.

the closest distance between the *t*-Bu group of the ligand and the coordinating diene or vinylogous lactone is 2.19 Å for either **TS1** or **TS2**, despite the fact that the experimentally observed 1,*x*- vs 4,1-regioselectivity (*t*Bu > *i*Pr > Me > H)[8] suggests a steric control. Analysis of the structures shown in Figure 6 reveals that the steric repulsion lead to an increase of the torsion angle between the two ring systems in the ligand (3.8° in **TS1** vs 12.2° in **TS2**) and a distortion of the palladium out of


DOI: 10.1021/acs.joc.6b01317
J. Org. Chem. 2016, 81, 7604−7611

the plane of the ligand (170.1° vs 152.8° relative to the plane of the oxazoline ring in **TS1** and **TS2**, respectively). This distortion of the ligand environment leads to the calculated energy difference between the two transition structures and the experimentally observed steric control of the 1,*x*- vs 4,1-selectivity.

**1,4- vs 1,2-Addition.** As outlined in Figure 5, **INT3** can lead to either the 1,4- or 1,2-addition product through $\sigma-\pi-\sigma$ ($\eta^1-\eta^3-\eta^1$) isomerization of the $\pi$-allyl-stabilized Pd-species. Due to the large number of possible isomers, we initially studied this reaction for the simplified model system shown in Figure 7. For this model, the $\sigma-\pi$-allyl ($\eta^1-\eta^3$) isomerization is

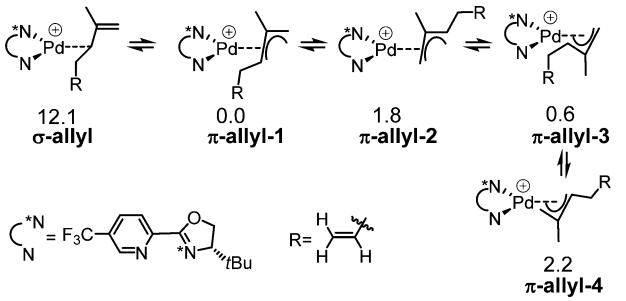


**Figure 7.** $\sigma-\pi$-Allyl isomerization and possible conformations of Pd-$\pi$-allyl complex.

exergonic by 12.1 kcal/mol. It should also be noted that there are four possible, rapidly interconverting Pd-$\pi$-allyl conformations. ***π*-Allyl-1** is found to be the most favorable conformation due to the minimization of steric interactions and will be used as the starting point for further discussion.

The subsequent cross-coupling sequence requires isomerization of the Pd-$\pi$-allyl complex (***π*-allyl-1**) to the reactive $\sigma$-allyl species, which then undergoes transmetalation with styrenylboronic acid. In this study, the styrenylboronic acid is represented by alkenyl boronic acid (ABA), and hydroxide is used as the base to facilitate transmetalation, in accordance with previous studies.[24−26] Due to the asymmetry of the bidentate pyrox ligand, there are four possible conformations for the hydroxide to coordinate to the palladium. Two of these conformations lead to Pd−$C_4$ bond formation, and the other two conformations lead to Pd−$C_2$ bond formation. In total, eight intermediates shown in Figure 8 need to be considered for the isomerization of ***π*-allyl-1**.

The relative energies of these eight intermediates can be rationalized by the modest *trans* effect of the hydroxyl group compared to the allylic carbanion and the enhanced *trans* effect of the oxazoline N compared to the pyridine N.[27] As a result, **C4_up** is more stable than **trans_C4_up**. In addition, **C4_down** is less stable than **trans_C4_down** due to the steric repulsion between the *t*-Bu group of the ligand and the adjacent allylic group.

To identify the rate and selectivity determining steps for the relevant conformations of the transition states leading to 1,4- and 1,2-addition products, the complete reaction pathway involving intermediate **C4_up** was calculated for the model system and is shown in Figure 9 (for additional, less favorable nucleophilic addition pathways, see Figure S2 in the Supporting Information). Starting from ***π*-allyl-1**, hydroxide-assisted $\pi-\sigma$-allyl isomerization forms **C4_up**, which is exergonic by 9.7 kcal/mol. Coordination of the alkenyl boronic acid to the hydroxyl group (**IN7**, $\Delta G$ = −6.6 kcal/mol) leads to **IN8** ($\Delta G$ = −7.9 kcal/mol). Following boronic acid coordination to hydroxide, a structural rearrangement to **IN9** with carbon−carbon double bond coordinating to Pd occurs via **TS3** with a barrier of 8.4 kcal/mol. The transmetalation step to form the stable intermediate **IN10** is irreversible with a free energy of reaction of $\Delta G$ = −26.9 kcal/mol. The transition structure **TS4** has a free energy of activation of 13.4 kcal/mol relative to **C4_up**. By releasing $B(OH)_3$, a more stable intermediate **IN11** ($\Delta G$ = −36.9 kcal/mol) is formed, mainly due to entropy gain. Reductive elimination via **TS5** to form the product-coordinated Pd(0) species (**IN12**) is again highly exergonic with a free energy of activation of 18.6 kcal/mol ($\Delta G$ = −60.4 kcal/mol).

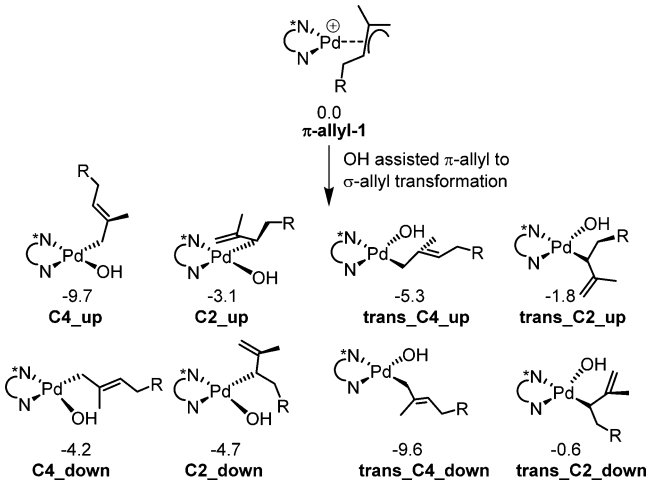


**Figure 8.** Hydroxide-assisted $\pi$-allyl to $\sigma$-allyl isomerization.

The transition structure for the transmetalation, **TS4**, determines the regioselectivity between 1,4- and 1,2-addition products by positioning the alkenyl boronic acid close to either the $C_4$ or $C_2$ position of the diene. Figure 10 shows the systematically enumerated conformational possibilities together with their calculated free energies relative to ***π*-allyl-1.** The structures where the alkenyl boronic acid is positioned *cis* to the pyridine portion of the ligand include **C4_cis1_TS4** to **C4_cis4_TS4**, which can be seen as different transition-state conformations derived from **C4_up**. Similarly, the structures where the alkenyl boronic acid is positioned *trans* to the pyridine portion of the ligand include **C4_trans1_TS4** to **C4_trans4_TS4**, which can be seen as different transition-state conformations derived from **trans_C4_down**, which is only 0.1 kcal/mol higher in energy than **C4_up** as shown in Figure 8. However, all transition structures **C4_trans1−4_TS4** are less stable than the corresponding **C4_cis1−4_TS4**, suggesting that the reaction pathway involving **trans_C4_down** is not as favorable as **C4_up** involved, though the two intermediates are only 0.1 kcal/mol difference in energy. The nomenclature for transition structures representing the addition to $C_2$ is analogous. We were unable to locate **C4_trans3_TS4** and **C2_trans3_TS4**, presumably due to the steric repulsion between $B(OH)_3$ and the *t*-Bu group of the ligand. The transition structures leading to the 1,4-addition products are in qualitative agreement with experimental observations, consistently lower in energy by at least ca. 1 kcal/mol.

Among the possible transition structures for attack at $C_4$ (top portion of Figure 10), the most favorable transition structure is **C4_cis3_TS4**, which has a free energy of activation of 3.7 kcal/mol relative to ***π*-allyl-1**. The transition structures for attack at $C_2$ (bottom portion of Figure 10) are calculated to be


DOI: 10.1021/acs.joc.6b01317
J. Org. Chem. 2016, 81, 7604−7611

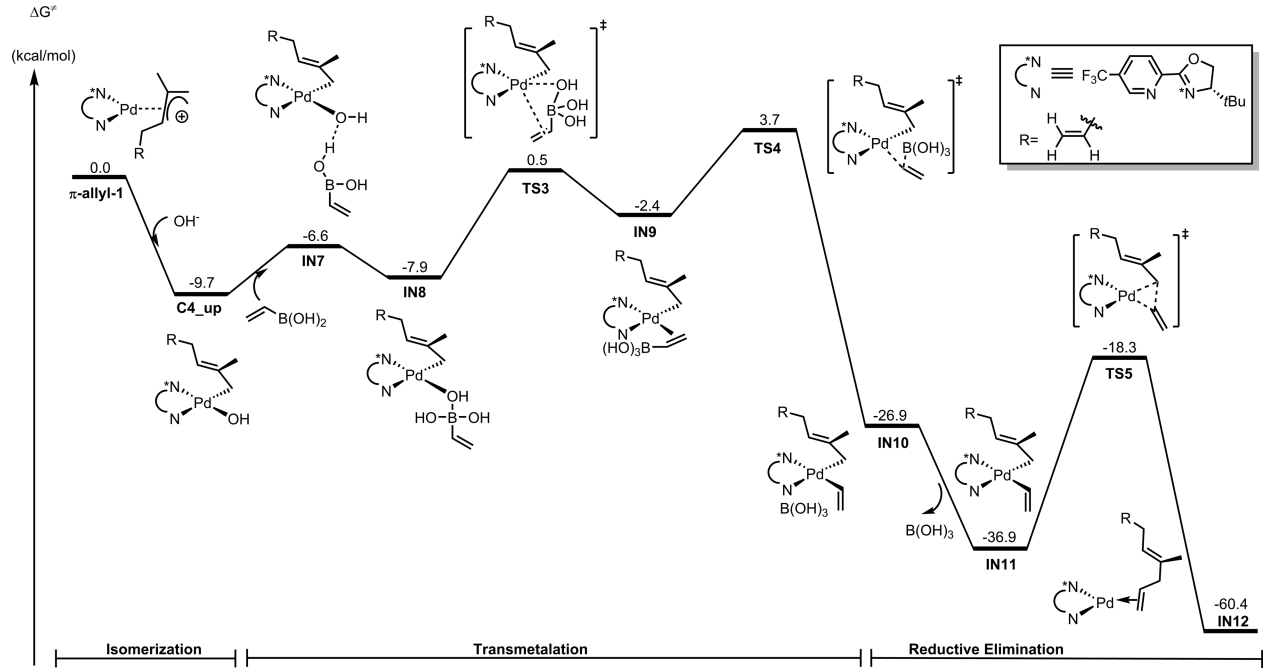


**Figure 9.** Potential energy surface for the 1,4-addition pathway.

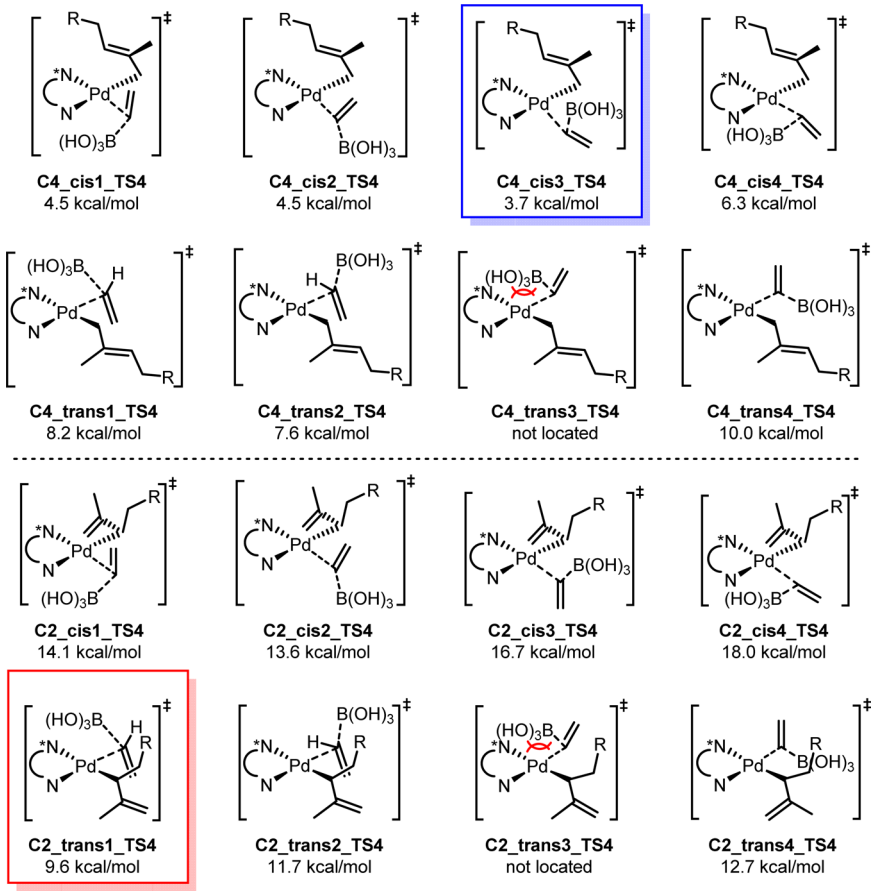


**Figure 10.** Possible conformations of **TS4** leading to 1,4- (**C4**) and 1,2-addition (**C2**) product formation.

consistently less favorable compared to the examples for attack at $C_4$ with the corresponding conformation. The transition structure for $C_2$ attack is **C2_cis3_TS2** (16.7 kcal/mol), which is much higher in energy than the corresponding to the lowest-energy transition structure at $C_4$, **C4_cis3_TS4**. Analysis of the transition structures reveals that in **C2_cis3_TS2**, the nearest H−H distance between the $C_2$-bound allylic group and the *t*-Bu substituent of the ligand is 1.93 Å, suggesting significant steric



DOI: 10.1021/acs.joc.6b01317
J. Org. Chem. 2016, 81, 7604−7611

repulsion (Figure 11). In comparison, there is no such unfavorable interaction in **C4_cis3_TS4**, as the $C_4$-bonded

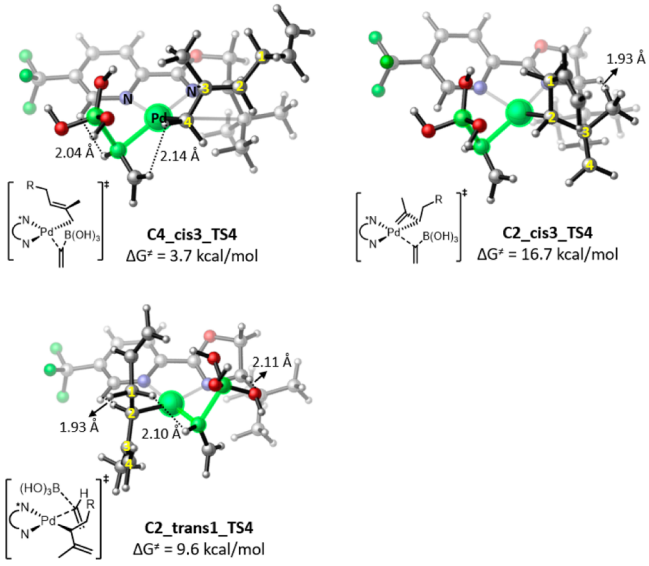


**Figure 11.** Transition structures **C4_cis3_TS4** and **C2_trans1_TS4**.

allylic group points away from the *t*-Bu substituent of the ligand. Systematic conformational searching indicates that **C2-trans1_TS4** has a free energy of activation of 9.6 kcal/mol relative to ***π*-allyl-1** and is the most favorable transition structure leading to $C_2$ (1,2-addition) selectivity. Therefore, the free energy of activation for the 1,2-addition model system is 5.9 kcal/mol higher than **C4_cis3_TS4** and is significantly greater than what would be expected from the low selectivity in observed the experimentally studied system.

Analysis of the structures involved and shown in Figure 12 reveals the origin of this energy difference. In the *trans* orientation in **C2_trans1_TS4**, where Pd is bound to $C_2$, steric repulsion between the substrate and pyridine ring of the ligand (nearest H−H distance: 1.93 Å) leads to an increase in energy. In addition, the steric interaction with the *t*-Bu of the ligand forces the alkenyl boronic acid toward the substrate. This promotes steric repulsion between the substrate and the alkenyl boronic acid (nearest H−H distance: 2.11 Å), further increasing the relative energy of **C2-trans1_TS4**. The structural analysis thus shows that, in agreement with the experimentally observed data, the 1,2- vs 1,4-selectivity is controlled by the interplay of steric repulsions between the *t*-Bu group on the ligand and the two substrates even if the energy difference is overestimated in the model system. A more quantitatively accurate description of this selectivity will therefore have to consider the steric bulk of the experimentally studied systems.

Starting with the lowest-energy conformations of the transition structures of the model system, structures of the corresponding **C4_cis1_TS4**, **C4_cis2_TS4**, **C4_cis3_TS4**, and **C2-trans1_TS4** were calculated for the experimentally studied system. As shown in Figure 12, the free energy difference between the $C_2$ and $C_4$ transition structures decreases to 4.9 kcal/mol in Figure 12, with **C4_cis1_TS4**

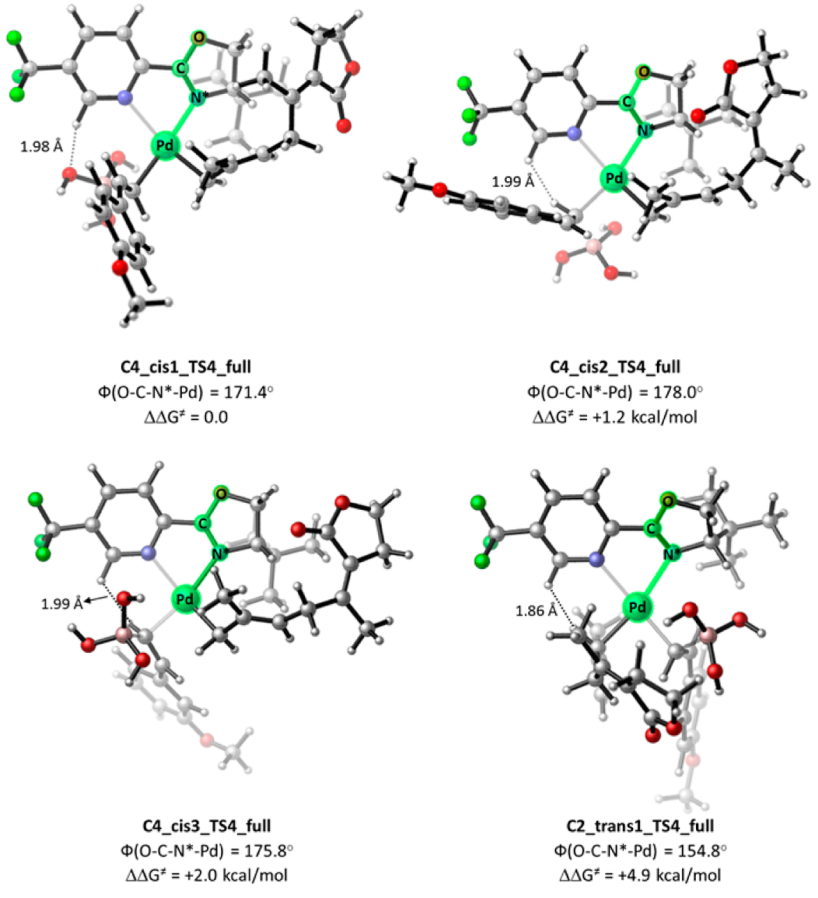


**Figure 12.** Geometries of **C4_cis1_TS4_full**, **C4_cis2_TS4_full**, **C4_cis3_TS4_full**, and **C2_trans1_TS4_full**.



DOI: 10.1021/acs.joc.6b01317
*J. Org. Chem.* 2016, 81, 7604−7611

being the most stable conformer among three $C_4$ transition structures. This is still an overestimation of the experimentally observed selectivity of 2.7:1,[8] but is a much better estimate based on a single geometry. More importantly, comparison of the structural details for the full system to the model system reveals the origin of the low experimentally observed selectivity. **C2_trans1_TS4_full** is subject to considerable steric strain, where the closest H−H distance between the styrenyl substrate and the pyridine ligand is only 1.86 Å. However, a similarly short distance of 1.99 Å is also observed in **C4_cis2_TS4_full** and **C4_cis3_TS4_full**, while in **C4_cis1_TS4_full**, steric strain between the substrate and the pyridine ligand is replaced by an attractive O−H interaction with a distance of 1.98 Å, which can explain why it is the most favorable $C_4$ transition structure conformation. In all cases, the steric effect leads to a distortion of palladium out of the plane of the ligand, with **C2_trans1_TS4_full** (154.8°) being more distorted than **C4_cis1_TS4_full** (171.4°), **C4_cis2_TS4_full** (178.0°), and **C4_cis3_TS4_full** (175.8°). Overall, steric effects between the substrate and the pyridine ligand account for the 1,4- versus 1,2-addition selectivity, although the differences are reduced in the experimentally studied system compared to the model system.

## CONCLUSIONS

The difunctionalization of isoprene catalyzed by palladium-pyrox complexes proceeds with moderate 1,*x*- vs 4,1-addition and 1,4- vs 1,2-addition selectivity. DFT calculations of the reaction pathway, including systematic conformational searches, were necessary for the description of this unsymmetrical three-component system. This analysis showed that the 1,*x*- vs 4,1-addition selectivity is set in the migratory insertion step and is controlled by steric repulsions that lead to a distortion of the palladium coordination sphere in the transition structure. Studies revealed that significant differences in the distances between substrate and the ligand were not responsible for 1,*x*- vs 4,1-addition regioselectivity. The calculated $\Delta\Delta G^{\ddagger}$ of 1.1 kcal/mol disfavoring the 4,1-addition product formation in a non-Curtin-Hammett scenario is in good agreement with the experimentally observed value of 9:9:1.

The selectivity-determining step for the 1,2- vs 1,4-addition pathways is computed to be the transmetalation. The relative stability of the relevant intermediates is controlled by a combination of *trans* effect of the pyrox ligand and steric influence of the ligands *t*-Bu group. A systematic search of the 16 possible conformations for the two possible transmetalation pathways identified the two lowest-energy transition structures for the model system, but overestimated the experimentally observed selectivity. Calculation of the nontruncated, experimentally studied system identified additional steric interactions responsible for the lowered 1,2- vs 1,4-addition regioselectivity, providing the structural basis for possible improvements of the selectivity for selected substrates, e.g., using the Q2MM approach.[28,29]

## ASSOCIATED CONTENT

### Supporting Information

The Supporting Information is available free of charge on the ACS Publications website at DOI: 10.1021/acs.joc.6b01317.

Additional computational data, including coordinates and energies for all described transition structures (PDF)

## AUTHOR INFORMATION


### Corresponding Author

*E-mail: owiest@nd.edu.

### Author Contributions

#These authors contributed equally.


### Notes

The authors declare no competing financial interest.

## ACKNOWLEDGMENTS

We thank the U.S. National Science Foundation (NSF CHE1058075), the National Science Foundation of China (NSFC 21133002), the Shenzhen Peacock Program (JCYJ20140509093817689), and the Nanshan District (KC2014ZDZJ0026A) for financial support. M.S.S. thanks the National Institute of Health (R01GM063540) for support.

## REFERENCES


(1) Sigman, M. S.; Werner, E. W. *Acc. Chem. Res.* **2012**, *45*, 874.
(2) Jensen, K. H.; Sigman, M. S. *Org. Biomol. Chem.* **2008**, *6*, 4083.
(3) McDonald, R. I.; Liu, G.; Stahl, S. S. *Chem. Rev.* **2011**, *111*, 2981.
(4) De Paolis, M.; Chataigner, I.; Maddaluno, J. *Top. Curr. Chem.* **2012**, *327*, 87.
(5) Liao, L.; Jana, R.; Urkalan, K. B.; Sigman, M. S. *J. Am. Chem. Soc.* **2011**, *133*, 5784.
(6) Liao, L.; Sigman, M. S. *J. Am. Chem. Soc.* **2010**, *132*, 10209.
(7) McCammant, M. S.; Liao, L.; Sigman, M. S. *J. Am. Chem. Soc.* **2013**, *135*, 4167.
(8) McCammant, M. S.; Sigman, M. S. *Chem. Sci.* **2015**, *6*, 1355.
(9) Stokes, B. J.; Liao, L.; de Andrade, A. M.; Wang, Q.; Sigman, M. S. *Org. Lett.* **2014**, *16*, 4666.
(10) Saini, V.; O'Dair, M.; Sigman, M. S. *J. Am. Chem. Soc.* **2015**, *137*, 608.
(11) Wu, X.; Lin, H.-C.; Li, M.-L.; Li, L.-L.; Han, Z.-Y.; Gong, L.-Z. *J. Am. Chem. Soc.* **2015**, *137*, 13476.
(12) Zhao, Y.; Truhlar, D. G. *Acc. Chem. Res.* **2008**, *41*, 157.
(13) Zhao, Y. T.; Truhlar, D. G. *Theor. Chem. Acc.* **2008**, *120*, 215.
(14) Frisch, M. J.; Trucks, G. W.; Schlegel, H. B.; Scuseria, G. E.; Robb, M. A.; Cheeseman, J. R.; Scalmani, G.; Barone, V.; Mennucci, B.; Petersson, G. A.; Nakatsuji, H.; Caricato, M.; Li, X.; Hratchian, H. P.; Izmaylov, A. F.; Bloino, J.; Zheng, G.; Sonnenberg, J. L.; Hada, M.; Ehara, M.; Toyota, K.; Fukuda, R.; Hasegawa, J.; Ishida, M.; Nakajima, T.; Honda, Y.; Kitao, O.; Nakai, H.; Vreven, T.; Montgomery, J. A., Jr.; Peralta, J. E.; Ogliaro, F.; Bearpark, M.; Heyd, J. J.; Brothers, E.; Kudin, K. N.; Staroverov, V. N.; Kobayashi, R.; Normand, J.; Raghavachari, K.; Rendell, A.; Burant, J. C.; Iyengar, S. S.; Tomasi, J.; Cossi, M.; Rega, N.; Millam, J. M.; Klene, M.; Knox, J. E.; Cross, J. B.; Bakken, V.; Adamo, C.; Jaramillo, J.; Gomperts, R.; Stratmann, R. E.; Yazyev, O.; Austin, A. J.; Cammi, R.; Pomelli, C.; Ochterski, J. W.; Martin, R. L.; Morokuma, K.; Zakrzewski, V. G.; Voth, G. A.; Salvador, P.; Dannenberg, J. J.; Dapprich, S.; Daniels, A. D.; Ö., Farkas, Foresman, J. B.; Ortiz, J. V.; Cioslowski, J.; Fox, D. J. *Gaussian 09*, Gaussian, Inc.: Wallingford, CT, 2009.
(15) Hilton, M. J.; Xu, L.-P.; Norrby, P.-O.; Wu, Y.-D.; Wiest, O.; Sigman, M. S. *J. Org. Chem.* **2014**, *79*, 11841.
(16) Xu, L.; Hilton, M. J.; Zhang, X.; Norrby, P.-O.; Wu, Y.-D.; Sigman, M. S.; Wiest, O. *J. Am. Chem. Soc.* **2014**, *136*, 1960.
(17) Nilsson Lill, S. O.; Ryberg, P.; Rein, T.; Bennström, E.; Norrby, P.-O *Chem. - Eur. J.* **2012**, *18*, 1640.
(18) Holder, J. C.; Zou, L.; Marziale, A. N.; Liu, P.; Lan, Y.; Gatti, M.; Kikushima, K.; Houk, K. N.; Stoltz, B. M. *J. Am. Chem. Soc.* **2013**, *135*, 14996.
(19) Hay, P. J.; Wadt, W. R. *J. Chem. Phys.* **1985**, *82*, 299.
(20) Ehlers, A. W.; Bohme, M.; Dapprich, S.; Gobbi, A.; Hollwarth, A.; Jonas, V.; Kohler, K. F.; Stegmann, R.; Veldkamp, A.; Frenking, G. *Chem. Phys. Lett.* **1993**, *208*, 111.




DOI: 10.1021/acs.joc.6b01317
J. Org. Chem. 2016, 81, 7604−7611

(21) Dolg, M.; Wedig, U.; Stoll, H.; Preuss, H. *J. Chem. Phys.* **1987**, *86*, 866.
(22) Marenich, A. V.; Cramer, C. J.; Truhlar, D. G. *J. Phys. Chem. B* **2009**, *113*, 6378.
(23) Legault, C. Y. *CYLview*; Université de Sherbrooke: Sherbrooke, Canada, 2009; http://www.cylview.org.
(24) Carrow, B. P.; Hartwig, J. F. *J. Am. Chem. Soc.* **2011**, *133*, 2116.
(25) Amatore, C.; Jutand, A.; Le Duc, G. *Chem. - Eur. J.* **2011**, *17*, 2492.
(26) Lennox, A. J. J.; Lloyd-Jones, G. C. *Angew. Chem., Int. Ed.* **2013**, *52*, 7362.
(27) McDonald, R. I.; White, P. B.; Weinstein, A. B.; Tam, C. P.; Stahl, S. S. *Org. Lett.* **2011**, *13*, 2830.
(28) Donoghue, P. J.; Helquist, P.; Norrby, P. O.; Wiest, O. *J. Chem. Theory Comput.* **2008**, *4*, 1313.
(29) Hansen, E.; Rosales, A. R.; Tutkowski, B. M.; Norrby, P. O.; Wiest, O. *Acc. Chem. Res.* **2016**, *49*, 996.



DOI: 10.1021/acs.joc.6b01317
*J. Org. Chem.* 2016, 81, 7604−7611